

Computations of Active Flow Control for Heavy Vehicle Drag Reduction

David E. Manosalvas-Kjono*, Thomas D. Economon,[†]
Stanford University, Stanford, CA, 94305, USA.

Carsten Othmer,[‡]
Volkswagen Group of America Inc., Belmont, CA 94002, USA.

and Antony Jameson[§]
Stanford University, Stanford, CA, 94305, USA.

This article aims to better understand the effect that Active Flow Control (AFC) drag reduction systems have in the aerodynamic profile of a Ground Transportation System (GTS) model when asymmetric blowing configurations are allowed. To that end, this study relies in the use of Reynolds-Averaged Navier-Stokes (RANS) to quantify the system effectiveness by simulating the flow over the vehicle and computing drag and overall power consumption. In this study the top, bottom, and the side jets blowing strengths are varied separately to quantify the effect of each component in the overall aerodynamic behavior of the vehicle. The wake structure and back pressure distribution for each blowing configuration have been analyzed, and the flow structure changes, due to asymmetric blowing, have been analyzed and turned into guidelines for future design studies of AFC drag reduction systems. This article shows that by allowing asymmetric blowing in the back of the GTS model, drag and power consumption have been reduced by 19% and 16% respectively.

I. Introduction and Motivation

Heavy vehicles drive our economy by helping mobilize goods within our country. These vehicles spend the majority of their life cycle at highway speeds (70 mph), at which over 65 % of the total energy consumed goes towards overcoming aerodynamic drag.¹ Using modern technologies to approach this problem, it has been shown that aerodynamic drag can be significantly reduced.¹ Achieving just a 12% reduction in fuel consumption across the national fleet of heavy vehicles would save 3.2 billion gallons of diesel per year and prevent the production of 28 million tons of CO_2 emissions.²

Flow separation and the development of low-pressure turbulent wakes are the main characteristics that can be used to describe the flow around a heavy vehicle.³ These combinations of features, which mainly occur in the trailer, are referred to as viscous pressure drag, or base drag, and are responsible for over 50% of the total vehicle drag.⁴ The resistance to motion caused by viscous pressure drag can be addressed by streamlining the vehicle, but due to the expected functionality of the trailer, a shape change in this area is not feasible. A non-intrusive approach for aerodynamic profile modification can be accomplished by the use of Active Flow Control (AFC) techniques, which operate by reducing the amount of separation behind the vehicle.⁵ These aerodynamic changes can be designed to reduce the pressure imbalance between the front and rear of the vehicle and through this avenue decreasing its drag.⁶ Coanda jet-based AFC systems positioned on the back of a heavy vehicle have been tested in wind tunnel experiments, and have proven

*Ph.D. Candidate, Department of Aeronautics & Astronautics, AIAA Student Member.

[†]Postdoctoral Scholar, Department of Aeronautics & Astronautics, AIAA Senior Member.

[‡]Senior Scientist and Project Lead, Electronics Research Laboratory; Stanford University Visiting Scholar, Department of Aeronautics & Astronautics.

[§]Research Professor, Department of Aeronautics & Astronautics, AIAA Fellow.

to be successful at maintaining the flow attached longer.⁵ AFC systems have demonstrated not only drag reduction, resulting in a net power savings of more than 15%, but also an improvement in vehicle stability and safety through the use of flow injection to compensate for the effect of side forces.³

For the effective design of AFC systems, it is necessary to understand the effects that each part of the system has on the flow features. Due to the complexity of the problem and appearance of separation, Large Eddy Simulation (LES) is believed to be the most reliable method when it comes to the simulation of these flows. Unfortunately, this approach increases the computational requirements significantly, making it prohibitively expensive for use in a design process, given current computational resources. In order to be able to use Computational Fluid Dynamics (CFD) for the design of AFC systems, it is necessary to use a combination of tools that will allow us to simulate the flow around heavy vehicles with an acceptable level of accuracy. In previous studies,⁶⁻⁸ the combination of Jameson-Schmidt-Turkel (JST)⁹ numerical scheme and the Shear-Stress-Transport (SST)¹⁰ turbulence model have been demonstrated as a good compromise between accuracy and computational cost for design purposes.

This article builds on the understanding that the Ground Transportation System (GTS) aerodynamic behavior is influenced by the ground, which stabilizes its wake.^{11,12} This behavior, in combination with the low frequency flow oscillations found by Khalighi *et al.*¹³ using Unsteady Reynolds-Averaged Navier-Stokes (URANS), justifies the use of Reynolds-Averaged Navier-Stokes (RANS) for the computation of integrated forces in a similar manner as the work presented by Roy *et al.*¹⁴ and Salari *et al.*¹⁵ This approach was used by the authors in 2016 and the integrated forces were in good agreement with experimental results.⁶ Furthermore, the lowest drag condition for the two-dimensional GTS model, outfitted with Coanda jets in the back, was shown to be achieved when the wake is confined and exhibits a steady behavior.^{7,8,16} The introduction of this type of AFC in the GTS model further justifies the use of RANS to investigate the effect that the jet strength has on the aerodynamic drag and power consumption of the vehicle.

This article aims to better understand the effect of asymmetric blowing configurations in the overall aerodynamic behavior and power consumption of the vehicle, and to achieve this goal the article is laid out as follows: in Section II the usefulness of the GTS model is explained and the justification for its use in this study is laid out. Section II-A presents a description of the GTS model outfitted with the Coanda jet AFC system and its geometry, introduces the flow conditions for the simulations, and defines the non-dimensional coefficients to be used throughout the study. Section II-B introduces the computational grid, the numerical tools used in the simulation, and the strategy used to model the jet flow injection. Section III provides a description of the full-factorial design study, introduces the strategies to visualize and analyze the results, and presents an analysis of the physical changes in the flow around the vehicle due to the variation of blowing configurations. Finally Section IV summarizes the results and shines some light in the direction where this work is going in the future.

II. Physical and Numerical Models

For the study of the aerodynamic features that characterize separated flows, and the quantification of the effects that add-on drag reduction devices have on the presence of viscous pressure drag, a streamlined model of a heavy vehicle is sufficient.^{4,17} Heavy vehicles have a variety of features that contribute towards flow separation, such as mirrors, antennas, gaps, mud flaps, etc., and to eliminate the effect that these have, the GTS¹⁷ model was used. This geometrical model was developed by a United States Department of Energy consortium to focus on the study of viscous pressure drag. The GTS effectively combines both the tractor and the trailer into a single simplified bluff body that has an elliptical leading shape and ends in a sharp straight cut in the back.¹⁷

A. Physical Geometry and Flow Conditions

This study is an extension of Manosalvas *et al.*,⁶ where a 6.5% scale model was used to study the effect of a Coanda jet based AFC drag reduction system in the aerodynamic profile of the vehicle. The enhanced GTS model, which is the base GTS model outfitted with the Coanda jet drag reduction system in the back, was used and can be seen in Figure 1.

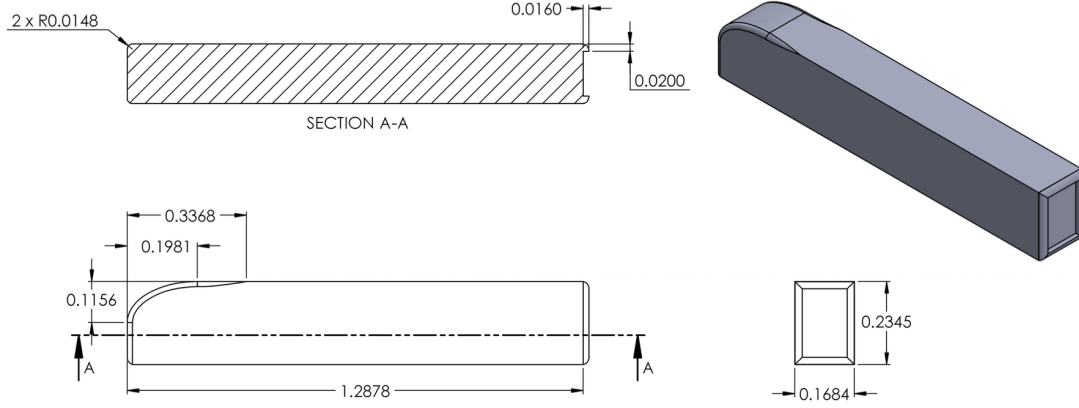


Figure 1: Three-dimensional GTS model with Coanda jets in the trailing edge - Scale 6.5%. All dimensions in meters.

The flow around the GTS model was simulated assuming standard air at sea-level treated as a calorically perfect ideal gas. The velocity was chosen to match the average highway speed, which is $31.3 \frac{m}{s}$ (70 mph) and translates to Mach number of 0.09195 and Reynolds number, using the GTS model width as the length scale, of 359,900.

The location of all four jets in the back of the GTS was selected to increase reattachment while limiting the interaction between jets. The size and spatial configuration of the jets were chosen based on the two-dimensional studies performed by the authors.^{7,8} For this study, spacing between the top of the jet and the roof of the GTS was eliminated, in an attempt to reduce grid complexity, allowing the jet to begin at the edge and have a thickness of $7.7978E - 4 m$ to maintain the Coanda surface geometry in accordance to the two-dimensional studies. The jet position can be seen in Figure 2. This configuration allows for the majority of the incoming flow to take advantage of high momentum air injection, which helps negotiate the sharp corners and reduces separation.

The effect of this GTS system was quantified by looking at the power required to overcome the aerodynamic drag combined with the power to energize the jets. The power used to overcome drag is defined as

$$P_{aero} = D * U_{\infty}, \quad (1)$$

where D is the aerodynamic drag and U_{∞} is the free-stream velocity. In addition, the power required to energize each Coanda jet is quantified by the change in kinetic energy of the injected fluid scaled by an efficiency factor to account for the losses of the system:

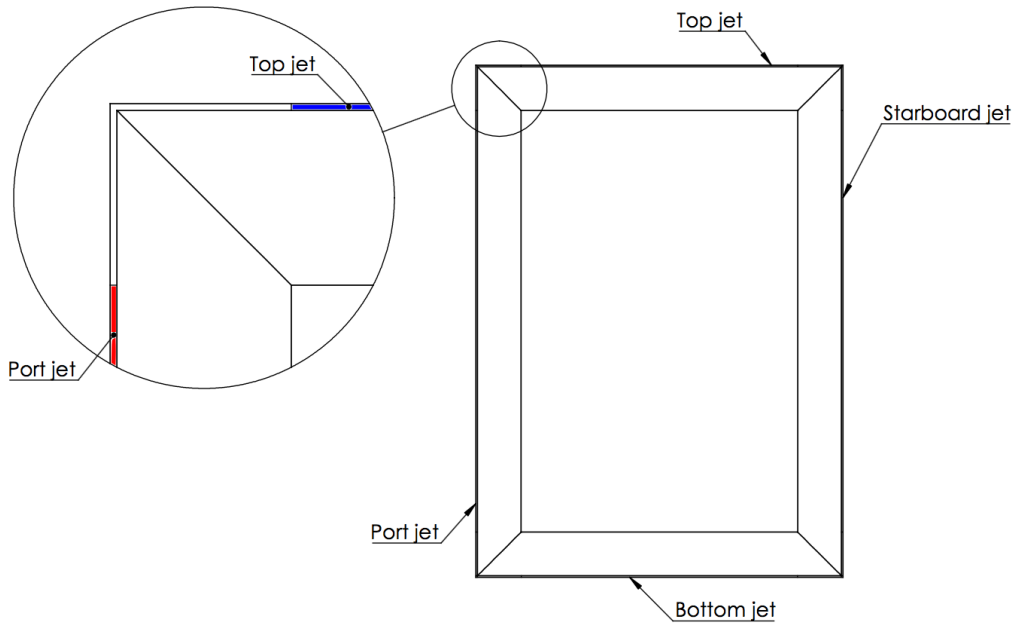
$$P_{comp} = \frac{\frac{1}{2} * \dot{m}_e * V_e^2}{\eta}, \quad (2)$$

where the mass flow rate through the jet is \dot{m}_e , V_e is the area-averaged jet velocity, and η is the efficiency factor, which was set to be 90% based on compressor isentropic efficiency values. For this study, the jets were modeled by imposing a velocity profile that was extracted from the two-dimensional results in previous work by the authors.⁸

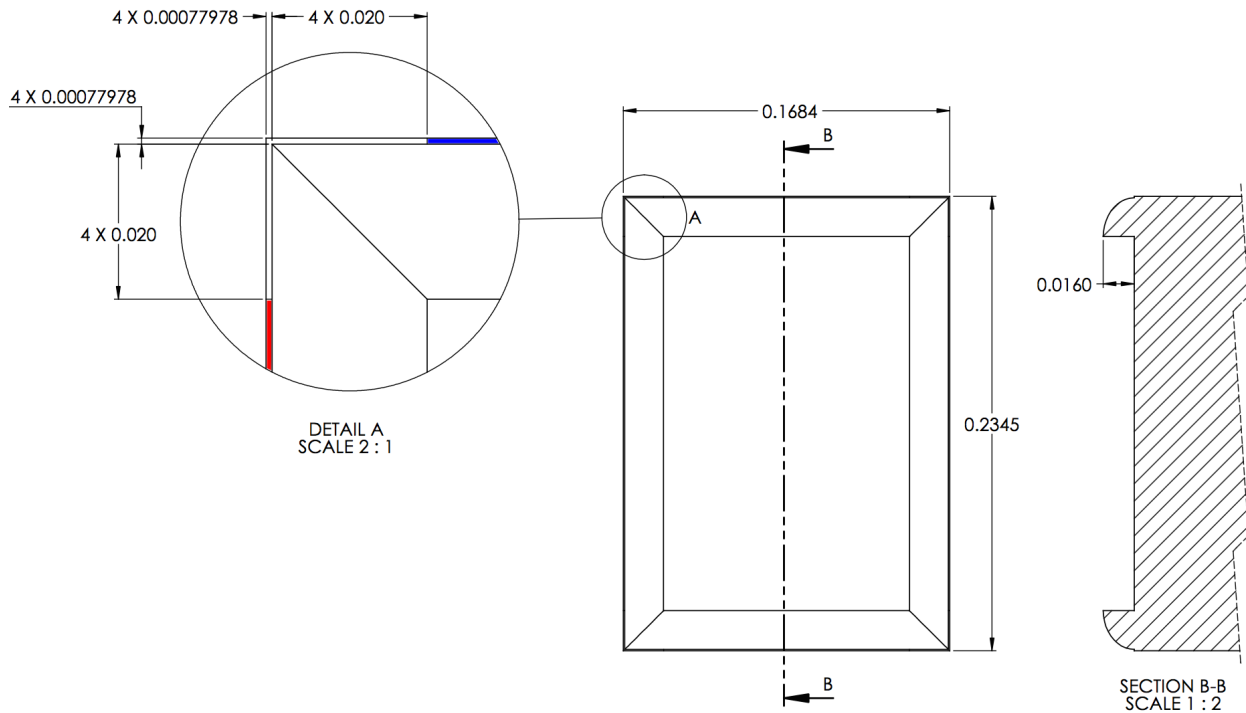
Non-dimensional coefficients for the drag, lateral forces, and lift have been defined as follows:

$$C_D = \frac{D}{q * A}, \quad C_{LF} = \frac{LF}{q * A}, \quad C_L = \frac{L}{q * A}, \quad (3)$$

where C_D is the drag coefficient, q is the dynamic pressure calculated as $\frac{1}{2} \rho_{\infty} U_{\infty}^2$, ρ_{∞} is the free-stream density, A is the cross-sectional area calculated as $W * H$, W is the width and H the height of the GTS model, C_{LF} is the lateral force coefficient, LF is the dimensional lateral force, C_L is the lift coefficient, and



(a) Jet configuration.



(b) Jet dimensions.

Figure 2: Coanda jets in the back of the enhanced GTS model - Scale 6.5%. In the detailed view the top jet is shown in red and the port jet in blue. All dimensions in meters.

L is the dimensional lift force. To characterize the jet strength and power consumption similar definitions are used:

$$C_\mu = \frac{\dot{m}_e * V_e}{q * A}, \quad C_{Pow} = \frac{P_{aero} + P_{comp}}{q * U_\infty * A}, \quad (4)$$

where C_μ is the momentum coefficient and C_{Pow} is the power coefficient.

B. Computational Domain and Numerical Tools

The computational grid that was used to represent the Coanda jet-equipped GTS geometry is fully unstructured with mixed element types. The boundary layer region is represented by prisms while the rest of the mesh is composed of tetrahedra. The mesh has 2,586,690 points, which corresponds to 11,112,620 cells. This grid was constructed guaranteeing that the y^+ remains below 1 and special emphasis was placed on refining the wake region, since this is the area of interest for the design of AFC systems. The grid can be seen in Figure 3.

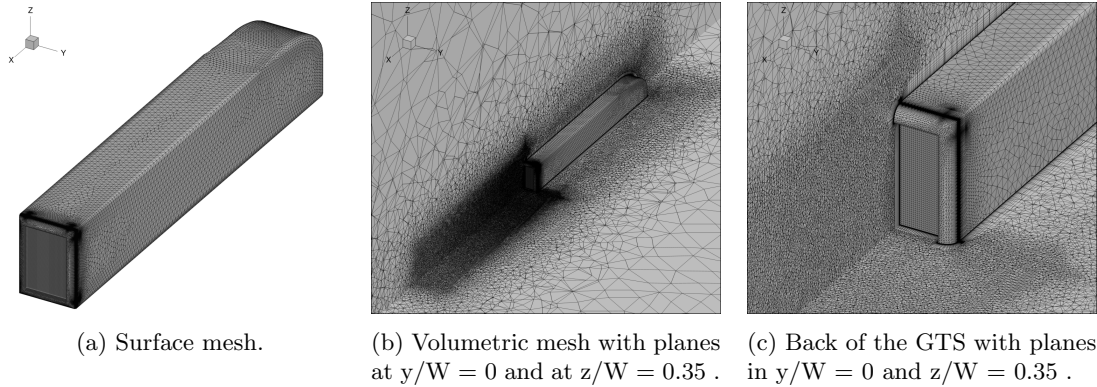


Figure 3: Grid for the GTS model with Coanda jets .

The GTS surface has been treated using an adiabatic no-slip condition. The far-field boundary of the domain is located in the axial direction at 5 truck lengths from the front and 9 truck lengths from the back. In the direction perpendicular to the flow, the vehicle is centered within 11 truck lengths, and in the direction normal to the ground, the domain spans 5 truck lengths. The outer domain boundaries are treated with the typical characteristic-based far-field condition for external aerodynamics. Finally, the ground plane is modeled using a slip condition, to avoid influencing the solution with the presence of a boundary layer.

To reduce the grid size and the computational resources required for this study, the jets were modeled through boundary conditions with specified velocity profiles, rather than modeling full plenums and nozzles internal to the vehicle. To recover proper behavior, these boundary conditions were implemented in SU2¹⁸⁻²⁰ as characteristic-based inlet conditions²¹ with both the velocity and density being specified on the jet face. The jet profiles have been modeled in accordance with the authors' 2016 study⁶ and for completeness can be seen as Equations 5 and 6 for the two-dimensionally mapped polynomial, and Equations 7, 8, 9, and 10 for the span-wise profile.

$$P_{bottom}^{top} = -0.7085458261471165 \tilde{z}^4 \pm 0.0082692314282440 \tilde{z}^3 - 0.2913746290723793 \tilde{z}^2 \mp 0.008259922266006 \tilde{z} + 0.9999361038208008, \quad (5)$$

$$\tilde{z} = \frac{z - z_{min}}{z_{max} - z_{min}} * 2 - 1, \quad (6)$$

where \tilde{z} is the mapped variable that goes from -1 to 1, z is the physical variable, and z_{max} and z_{min} are the physical limits between which the polynomial needs to be mapped.

$$\delta = \frac{0.382 W}{Re^{1/5}}, \quad (7)$$

$$Re = \frac{\rho_p * V_{peak} * W}{\mu_p}, \quad (8)$$

$$\mu_p = 1.716 * 10^{-5} \left[\frac{T_p}{273.15} \right]^{\frac{3}{2}} \left[\frac{273.15 + 110.4}{T_p + 110.4} \right], \quad (9)$$

where δ is the boundary layer thickness, W is the GTS model width, Re is the Reynolds number, ρ_p is the jet density calculated assuming the injected flow to be an ideal gas at $T_p = 290 \text{ K}$ and a pressure of $101,325 \text{ Pa}$, V_{peak} is the peak velocity of the jet, and μ_p is the jet viscosity computed using Sutherland's law.²²

$$R = \begin{cases} 1 - \frac{4}{4\delta^2} * (\tilde{y} + 1 - \tilde{\delta})^2 & \text{if } -1 < \tilde{y} < -1 + \tilde{\delta}, \\ 1 & \text{if } -1 + \tilde{\delta} < \tilde{y} < 1 - \tilde{\delta}, \\ 1 - \frac{4}{4\delta^2} * (\tilde{y} - 1 + \tilde{\delta})^2 & \text{if } 1 - \tilde{\delta} < \tilde{y} < 1. \end{cases} \quad (10)$$

For ease of implementation, both profiles are combined into a single function for which its magnitude is normalized:

$$M(z, y) = P(z) * R(y) * V_{peak}, \quad (11)$$

and a visual representation of it can be seen in Figure 4.

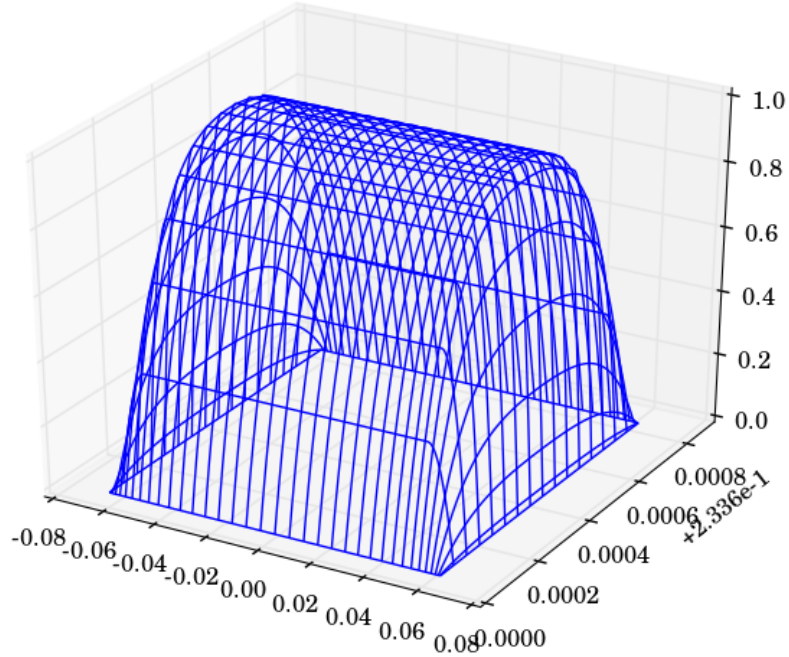


Figure 4: Normalized three-dimensional profile for the top jet.

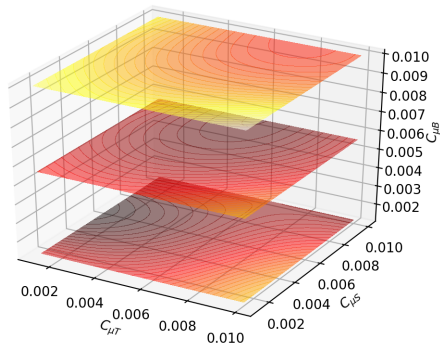
This study was performed following the guidelines established by the authors in 2016,⁶ where the flow around the vehicle is treated as a steady problem using the second-order accurate JST⁹ convective scheme and a corrected average of gradients viscous scheme²³ for the mean flow, in combination with the SST¹⁰ turbulence model.

III. Numerical Experiments and Results

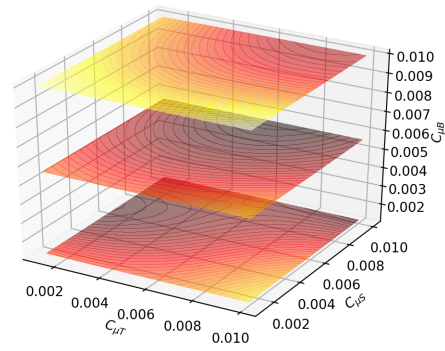
To properly design AFC systems capable of significantly reducing harmful emissions and vehicle energy consumption, it is important to understand the effects that jet injection strength has on the overall aerodynamic behavior of the vehicle. In 2016, the authors showed that a 12% power reduction can be achieved by varying the momentum coefficient of all jets as a single variable.⁶ This study leveraged on the understanding of ground effect and its stabilizing influence in the wake behavior,^{11, 12} which in addition to allowing for the reduction of computational costs, unveiled the need for jet specific momentum coefficients. The introduction of these new variables opens the design space to the existence of new power coefficient extrema, which can be found by better understanding the physics behind aerodynamic modifications. Due to symmetry, the port and starboard jets, also deferred as side jets, can be controlled using a single parameter, but the top and bottom jets need to be controlled individually.

<i>Case</i>	$C_{\mu B}$	$V_{PBottom}$	$C_{\mu T}$	V_{PTop}	$C_{\mu S}$	V_{PSide}	C_D	C_{Pow}
[—]	[—]	$[\frac{m}{s}]$	[—]	$[\frac{m}{s}]$	[—]	$[\frac{m}{s}]$	[—]	[—]
1	0.001250	20.8997	0.001250	20.8997	0.001250	16.8732	0.3032	0.3044
2	0.001250	20.8997	0.001250	20.8997	0.005625	35.7443	0.2727	0.2788
3	0.001250	20.8997	0.001250	20.8997	0.010000	47.6366	0.2852	0.2987
4	0.001250	20.8997	0.005625	44.2461	0.001250	16.8732	0.3053	0.3095
5	0.001250	20.8997	0.005625	44.2461	0.005625	35.7443	0.2856	0.2947
6	0.001250	20.8997	0.005625	44.2461	0.010000	47.6366	0.2781	0.2945
7	0.001250	20.8997	0.010000	58.9541	0.001250	16.8732	0.3252	0.3340
8	0.001250	20.8997	0.010000	58.9541	0.005625	35.7443	0.3060	0.3196
9	0.001250	20.8997	0.010000	58.9541	0.010000	47.6366	0.2726	0.2936
10	0.005625	44.2461	0.001250	20.8997	0.001250	16.8732	0.3078	0.3121
11	0.005625	44.2461	0.001250	20.8997	0.005625	35.7443	0.2907	0.2998
12	0.005625	44.2461	0.001250	20.8997	0.010000	47.6366	0.2857	0.3021
13	0.005625	44.2461	0.005625	44.2461	0.001250	16.8732	0.3050	0.3122
14	0.005625	44.2461	0.005625	44.2461	0.005625	35.7443	0.2806	0.2926
15	0.005625	44.2461	0.005625	44.2461	0.010000	47.6366	0.2673	0.2867
16	0.005625	44.2461	0.010000	58.9541	0.001250	16.8732	0.3233	0.3351
17	0.005625	44.2461	0.010000	58.9541	0.005625	35.7443	0.2919	0.3085
18	0.005625	44.2461	0.010000	58.9541	0.010000	47.6366	0.2777	0.3017
19	0.010000	58.9541	0.001250	20.8997	0.001250	16.8732	0.3411	0.3499
20	0.010000	58.9541	0.001250	20.8997	0.005625	35.7443	0.3251	0.3387
21	0.010000	58.9541	0.001250	20.8997	0.010000	47.6366	0.3200	0.3410
22	0.010000	58.9541	0.005625	44.2461	0.001250	16.8732	0.3319	0.3437
23	0.010000	58.9541	0.005625	44.2461	0.005625	35.7443	0.3063	0.3229
24	0.010000	58.9541	0.005625	44.2461	0.010000	47.6366	0.2910	0.3150
25	0.010000	58.9541	0.010000	58.9541	0.001250	16.8732	0.3486	0.3649
26	0.010000	58.9541	0.010000	58.9541	0.005625	35.7443	0.3056	0.3267
27	0.010000	58.9541	0.010000	58.9541	0.010000	47.6366	0.2874	0.3159

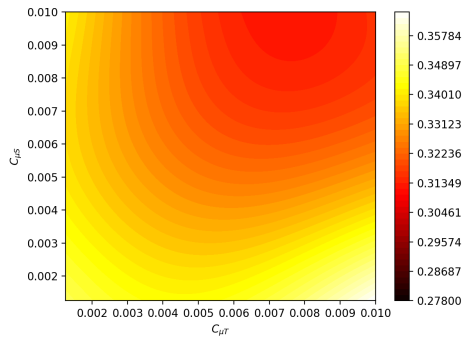
Table 1: Blowing strength configurations and resulting drag and power coefficients for the full-factorial study of a GTS model outfitted with the AFC system. $C_{\mu B}$ is the bottom jet momentum coefficient, $V_{PBottom}$ is the peak velocity on the bottom jet, $C_{\mu T}$ is the top jet momentum coefficient, V_{PTop} is the peak velocity on the top jet, $C_{\mu S}$ is the momentum coefficient on each of the side jets, V_{PSide} is the peak velocity on each of the side jets, C_D is the drag coefficient and C_{Pow} is the power coefficient.



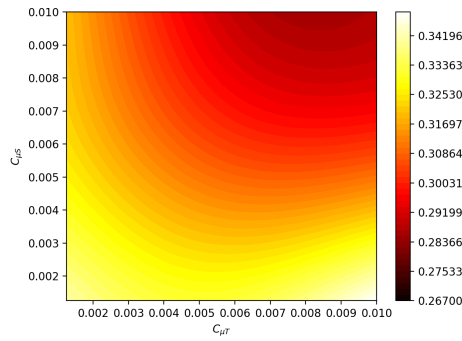
(a) Design Space - C_{Pow}



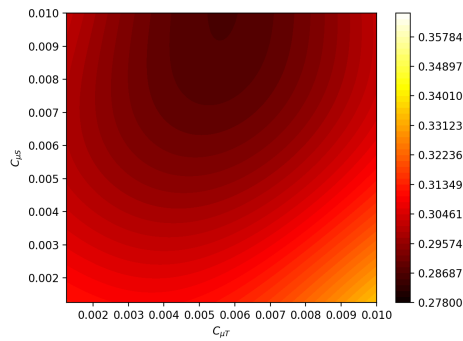
(b) Design Space - C_D



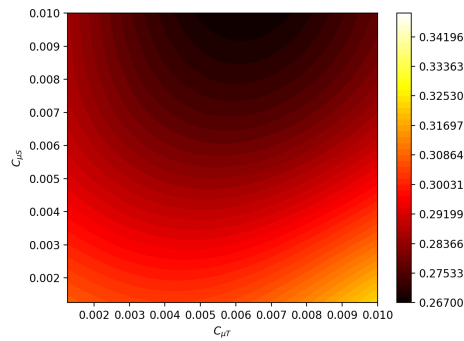
(c) $C_{\mu B} = 0.01$



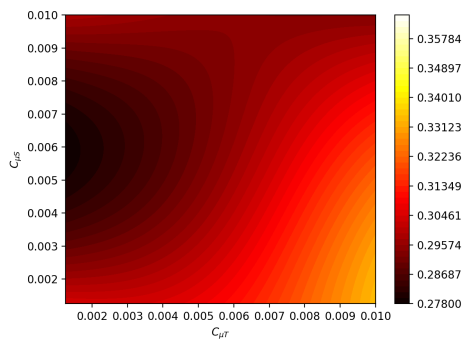
(d) $C_{\mu B} = 0.01$



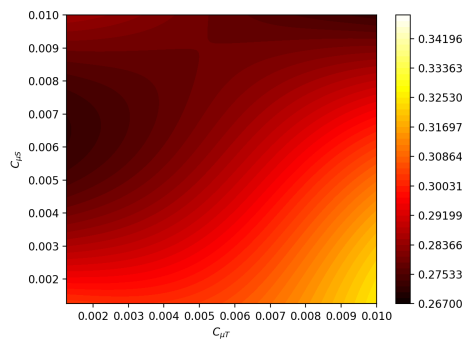
(e) $C_{\mu B} = 0.005625$



(f) $C_{\mu B} = 0.005625$



(g) $C_{\mu B} = 0.00125$



(h) $C_{\mu B} = 0.00125$

Figure 5: Surrogate models of the power coefficient in the left column (a, c, e, g) and the drag coefficient in the right column (b, d, f, h) for the full-factorial study at different bottom jet momentum coefficient values.

To span the design space, a full-factorial study was put in place, where each momentum coefficient (C_μ) is allowed to vary between 0.00125, 0.005625 and 0.01. The 27 function evaluations that result from the permutation of these blowing coefficients can be seen in Table 1. The peak velocities shown in Table 1 are inversely proportional to the corresponding jet area. Therefore, the peak velocity differences at a given C_μ between top, bottom, and side jets are due to this feature.

To better interpret the results obtained from this study, the data has been split in three groups keeping the bottom jet momentum coefficient ($C_{\mu B}$) constant for each group due to its direct relation with ground effect. Each group is conformed by 9 sample points which are evenly distributed. The design spaces for both the power and drag coefficients at each of the $C_{\mu B}$ levels were assumed to be continuous, and have been represented using surrogate models. These response surfaces have been generated using Gaussian Process Regression (GPR) techniques, and a square exponential kernel was chosen to build the surrogate models.²⁴ The open source python library Scikit-learn²⁵ implementation of this technique was used to generate the response surfaces and the resulting design space representations can be seen in Figure 5.

The aerodynamic analysis required to better understand the physical changes of the wake, and the overall vehicle aerodynamic behavior, has been performed by using two-dimensional cuts of the flow behind the GTS.^{26,27} One vertical and two horizontal slices have been used to study the wake structure changes induced by the AFC system and their locations can be seen in Figure 6.

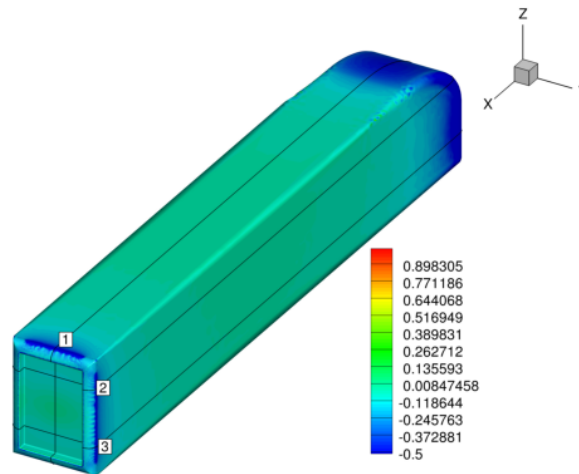


Figure 6: Location of the slices used to study the wake GTS model outfitted with a Coanda based AFC system. (1) is a vertical slice located at $y/W = 0$, (2) is a horizontal slice located at $z/W = 1.05$ and (3) is a horizontal slice placed at $z/W = 0.35$. Pressure coefficient is shown in the vehicle's surface.

Starting from Figures 5c and 5d, it is clear that the power consumption of the system, and the drag generated by the vehicle, are at the highest levels when the bottom jet operates at full strength and is trying to counteract the ground effect. Case 25 exhibits the highest power and drag coefficients with values of 0.3649 and 0.3486 respectively. This configuration was obtained by blowing the top and bottom jets at full strength ($C_\mu = 0.01$), while the side jets were operated at the minimum strength ($C_\mu = 0.00125$). The bottom jet propels the flow from under the body upwards and shifts the wake's tail above the vertical centerline. At the mean time, the top jet attempts to push the wake back down, but due to its interaction with the external flow coming from the top of the vehicle, the top jet effect on the wake is further downstream. The interaction between the top and bottom jets gives rise to an asymmetric pair of counter rotating horizontal vortices that are pushed towards the back of the truck, as can be seen in Figure 7b. The overwhelming effect of the top and bottom jets can be better appreciated by looking at the normalized ground-normal velocity magnitude in Figures 7c and 7d. Furthermore, these Figures show a pair of vertical counter rotating vortices that span the height of the GTS model and have been forced outside of the top and bottom jet's influence region. The side jets struggle to constrain the position of these vortical structures and allow a thick wake to form. The position of these vortices gives rise to intermittent smaller vortices in the back of the truck, and their interaction causes a low and asymmetric back pressure distribution, as can be seen in Figure 7a.

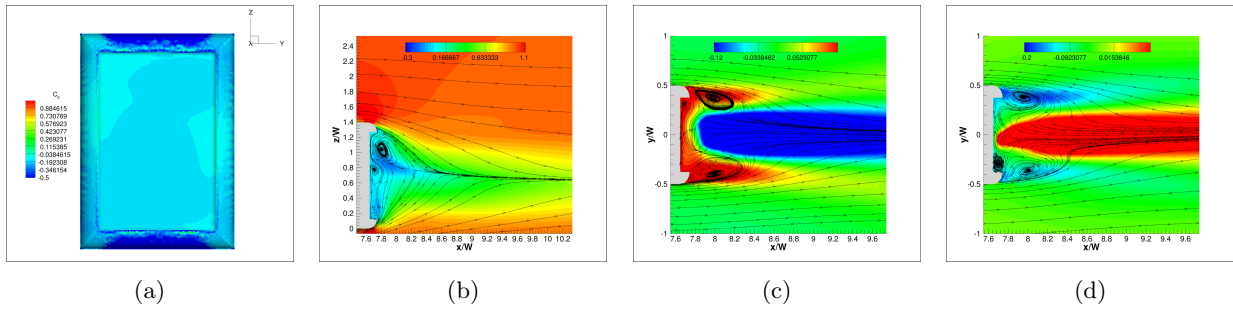


Figure 7: Wake structure and pressure distribution of the flow triggered by the blowing configuration of case 25. (a) shows the back pressure coefficient, (b) is slice 1 showing a contour of the normalized stream-wise velocity, (c) is slice 2 showing a contour of the normalized ground-normal velocity, and (d) is slice 3 showing a contour of the normalized ground-normal velocity.

To reduce the effect of the vertical vortices in case 25, the blowing strength of the side jets has been increased to its maximum setting. This configuration is represented in case 27, where both the power and drag coefficients decreased to 0.3159 and 0.2874 respectively. In this configuration the wake is fully restrained, and its behavior is driven by the top and bottom jets, which establish a pair of counter-rotating horizontal vortices. The introduction of high momentum flow from the side jets constrains the wake laterally and influences the ground-normal behavior by giving it a quasi-symmetric structure, as can be seen in Figure 8b. Furthermore, the side jets significantly decrease the presence of vertical vortices, as shown in Figures 8c and 8d, and allow for a significant increase of the back pressure, shown in Figure 8a. The presence for high momentum jet flow in this configuration counteracts the pressure increase in the back of the vehicle, by inducing low pressures in the Coanda surfaces, which despite the aerodynamic improvements in the wake causes the drag to stagnate. The power required to energize the AFC system in this configuration is significantly higher and its power signature drives the system behavior despite the drag improvements.

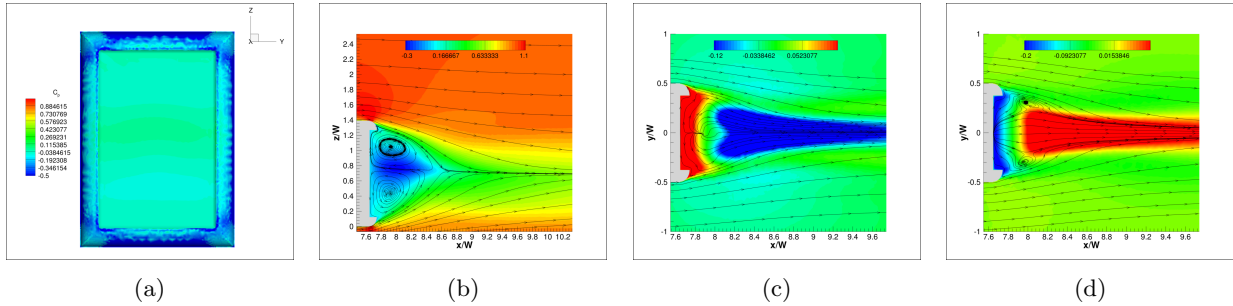


Figure 8: Wake structure and pressure distribution of the flow triggered by the blowing configuration of case 27. (a) shows the back pressure coefficient, (b) is slice 1 showing a contour of the normalized stream-wise velocity, (c) is slice 2 showing a contour of the normalized ground-normal velocity, and (d) is slice 3 showing a contour of the normalized ground-normal velocity.

By reducing the strength of the bottom and top jets to the mid-level ($C_{\mu} = 0.005625$), while maintaining the side jets at a high blowing strength, the GTS drag and power coefficients decrease. Case 15 uses this configuration and, as can be seen in Figures 9b, 9c, and 9d, the dominance of the horizontal vortices is decreased as the vertical vortices reappear. The recirculating nature of the wake is represented as a torus of revolution with a coplanar axis positioned parallel to the flow stream direction and normal to the back of the GTS. The bottom jet counteracts the ground effect and pushes the wake's tail closer to the centerline. This wake structure significantly increases the pressure in the back face of the GTS, as can be seen in Figure 9a, and the drag coefficient obtained is the global minimum with a value of 0.2673. The power coefficient required to maintain this wake configuration is 0.2867.

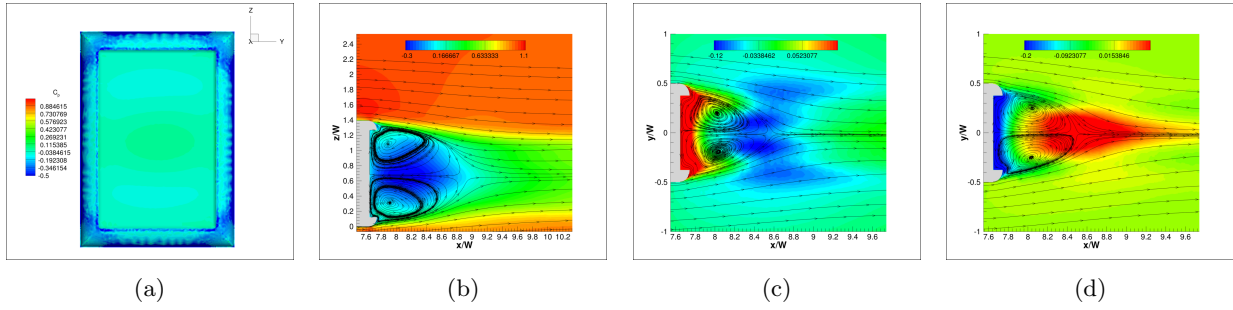


Figure 9: Wake structure and pressure distribution of the flow triggered by the blowing configuration of case 15. (a) shows the back pressure coefficient, (b) is slice 1 showing a contour of the normalized stream-wise velocity, (c) is slice 2 showing a contour of the normalized ground-normal velocity, and (d) is slice 3 showing a contour of the normalized ground-normal velocity.

Although case 15 represented the minimum drag coefficient in the study, the minimum power coefficient was achieved in case 2, where the top and bottom jets are blowing at the minimum momentum coefficient, and the side jets at the mid-level. This case is analogous to case 15 but at a lower blowing level for all jets. The wake behavior under this blowing configuration is similar to the one described in case 15, where both horizontal and vertical vortices interact and behave as a torus of revolution. The tail of the wake is closer to the ground since the bottom jet is doing less work against the ground effect, which introduces a slight vertical asymmetry and can be seen in Figure 10b. In addition, the wake is longer in this configuration and, due to the lower overall momentum coefficient, is wider and allows for a lower back pressure, when compared to case 15, as can be clearly seen in Figures 10a, 10c and 10d. The reduced jet flow velocity contributes to the presence of higher pressure in the Coanda surfaces, preventing a sharp increase in drag, and requires less power to energize the system, which makes this configuration the most power efficient in this study. The power and drag coefficients for this configuration are 0.2788 and 0.2727 respectively, which compared to the base GTS model power coefficient of 0.3323⁶ produce an improvement of 16.1% in power consumption.

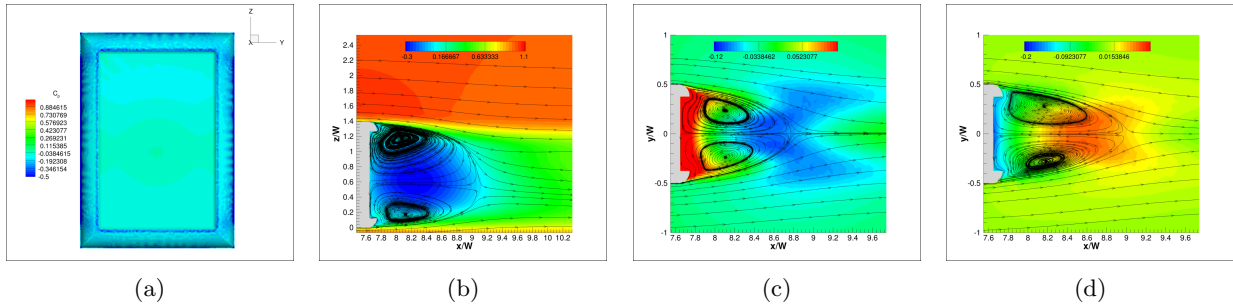


Figure 10: Wake structure and pressure distribution of the flow triggered by the blowing configuration of case 2. (a) shows the back pressure coefficient, (b) is slice 1 showing a contour of the normalized stream-wise velocity, (c) is slice 2 showing a contour of the normalized ground-normal velocity, and (d) is slice 3 showing a contour of the normalized ground-normal velocity.

IV. Conclusion and Future Work

This article used the numerical setup introduced by the authors in 2016⁶ to simulate the aerodynamic profile of a GTS model outfitted with a Coanda jet based AFC drag reduction system. To better understand the system's influence in the power consumption and vehicle's aerodynamic drag, jet specific momentum coefficients were used. Due to symmetry the port and starboard jets, also referred to as side jets, were controlled together, while the top and bottom jets were allowed to vary separately.

To span the design space, a full-factorial study using 27 sampling configurations was used. The momentum coefficients were allowed to vary between 0.00125, 0.005625, and 0.01; and all combinations of these

parameters were studied. The drag and power consumption resulting from these simulations were visualized by dividing the data set into 3 groups of 9 function evaluations each, where the bottom jet momentum coefficient was kept constant, and surrogate models of each group were generated using GPR methods.

Using the surrogate models to guide the exploration, four cases were selected to highlight the effect the AFC system had in the wake structure and performance of the vehicle. In case 25, the jets manipulate the wake to increase the drag of the vehicle by making the wake unstable. Although this behavior is consistent with the results reported in the literature,^{5,7,8} an accurate simulation of this configuration using unsteady methods is required. Case 27 increases the side jets strength to restrain the wake and improves its stability, but a combination of low Coanda surface pressure and high power consumption guide the selection to a more conservative blowing approach. Case 15 is shown to restrain the wake and is able to reduce drag by 19.6%, which gives the minimum drag value of this study. This configuration requires a significant amount of blowing and therefore a compromise on drag is required to find the minimum power consumption configuration. Case 2 is a low-blowing analogous of case 15, where the wake is controlled in a similar manner, but by compromising in drag minimization, it achieves the minimum power usage seen in this study with a 16.1% power and 17.9% drag reduction.

In the future we aim to understand the effect of higher Reynolds numbers in the performance of AFC drag reduction systems. We plan to perform higher fidelity simulations using Detached Eddy Simulation (DES) to confirm the optimum configuration obtained with these computationally inexpensive tools, and to validate the design by using experimental data. In addition, we would like to investigate the potential to increase the system performance by Coanda surface shape optimization.

V. Acknowledgments

The authors would like to thank the Stanford Vice Provost for Graduate Education, and the Ford Foundation for their support; the Extreme Science and Engineering Discovery Environment (XSEDE)²⁸ under grant number TG-ENG160027, which is supported by National Science Foundation (NSF) grant number ACI-1053575, for the computational resources required to make this study possible; the members of the Aerospace Computing Laboratory and the Aerospace Design Laboratory at Stanford University for many useful discussions, and the SU2 development team for their hard work maintaining this open source CFD suite.

References

- ¹McCallen, R., Flowers, D., Dunn, T., Owens, J., Browand, F., Hammache, M., Leonard, A., Brady, M., Salari, K., Rutledge, W., Ross, J., Storms, B., Heineck, J., Driver, D., Bell, J., Walker, S., and Zilliac, G., "Aerodynamic Drag of Heavy Vehicles (Class 7-8): Simulation and Benchmarking," *SAE Technical Paper Series*, 2000.
- ²McCallen, R., Salari, K., Ortega, J., DeChant, L., Hassan, B., Roy, C., Pointer, W. D., Browand, F., Hammache, M., Hsu, T., Leonard, A., Rubel, M., Chatelain, P., Englar, R. J., Ross, J., Satran, D., Heineck, J., Walker, S., Yaste, D., and Storms, B., "DOE's Effort to Reduce Truck Aerodynamic Drag - Joint Experiments and Computations Lead to Smart Design," *34th AIAA Fluid Dynamics Conference and Exhibit*, jun 2004.
- ³Pfeiffer, J. and King, R., "Multivariable Closed-Loop Flow Control of Drag And Yaw Moment For A 3D Bluff Body," *6th AIAA Flow Control Conference*, jun 2012.
- ⁴van Leeuwen, P. M., *Computational Analysis of Base Drag Reduction Using Active Flow Control*, Ph.D. thesis, Delft University of Technology, nov 2009.
- ⁵Englar, R. J., "Advanced aerodynamic devices to improve the performance, economics, handling, and safety of heavy vehicles," *SAE Technical Paper Series*, 2001.
- ⁶Manosalvas, D. E., Economon, T. D., Othmer, C., and Jameson, A., "Computational Design of Drag Diminishing Active Flow Control Systems for Heavy Vehicles," *8th AIAA Flow Control Conference*, American Institute of Aeronautics and Astronautics, Reston, Virginia, jun 2016.
- ⁷Manosalvas, D. E., Economon, T. D., Palacios, F., and Jameson, A., "Finding Computationally Inexpensive Methods to Model the Flow Past Heavy Vehicles and the Design of Active Flow Control Systems for Drag Reduction," *32nd AIAA Applied Aerodynamics Conference*, jun 2014.
- ⁸Manosalvas, D. E., Economon, T. D., Palacios, F., and Jameson, A., "Techniques for the Design of Active Flow Control Systems in Heavy Vehicles," *33rd AIAA Applied Aerodynamics Conference*, jun 2015.
- ⁹Jameson, A., Schmidt, W., and Turkel, E., "Numerical solution of the Euler equations by finite volume methods using Runge Kutta time stepping schemes," *AIAA paper*, jun 1981.
- ¹⁰Menter, F. R., "Two-equation eddy-viscosity turbulence models for engineering applications," *AIAA Journal*, Vol. 32, No. 8, aug 1994, pp. 1598–1605.
- ¹¹Kim, T., Lee, B., Lee, D., Lee, D., Hwang, J., and Lee, D., "A Study on Vortex Shedding Around a Bluff Body Near the Ground," *SAE Technical Paper Series*, 2003.

- ¹²Agarwal, R., “Computational study of drag reduction of models of truck-shaped bodies in ground effect by active Flow control,” *SAE Technical Paper Series*, 2013.
- ¹³Khalighi, B., Zhang, S., Koromilas, C., Balkanyi, S. R., Bernal, L. P., Iaccarino, G., and Moin, P., “Experimental and Computational Study of Unsteady Wake Flow Behind a Bluff Body with a Drag Reduction Device,” *SAE Technical Paper Series*, 2001.
- ¹⁴Roy, C., Payne, J., and McWherter-Payne, M., “RANS Simulations of a Simplified Tractor/Trailer Geometry,” *Journal of Fluids Engineering*, Vol. 128, 2006, pp. 1083.
- ¹⁵Salari, K., Ortega, J., and Castellucci, P., “Computational Prediction of Aerodynamic Forces for a Simplified Integrated Tractor-Trailer Geometry,” *34th AIAA Fluid Dynamics Conference and Exhibit*, American Institute of Aeronautics and Astronautics, Reston, Virginia, jun 2004.
- ¹⁶Englar, R. J., “Improved Pneumatic Aerodynamics for Drag Reduction, Fuel Economy, Safety and Stability Increase for Heavy Vehicles,” *SAE Technical Paper Series*, nov 2005.
- ¹⁷Gutierrez, W. T., Hassan, B., and Robert, H., “Aerodynamics Overview of the Ground Transportation Systems (GTS) Project for Heavy Vehicle Drag Reduction,” *SAE International Congress and Exposition*, 1996.
- ¹⁸Economon, T. D., Palacios, F., Copeland, S. R., Lukaczyk, T. W., and Alonso, J. J., “SU2: An Open-Source Suite for Multiphysics Simulation and Design,” *AIAA Journal*, Vol. 54, No. 3, 2015, pp. 828–846.
- ¹⁹Palacios, F., Economon, T. D., Aranake, A., Copeland, S., Lonkar, A., Lukaczyk, T., Manosalvas, D. E., Naik, K., Padron, A. S., Tracey, B., Variyar, A., and Alonso, J. J., “Stanford University Unstructured (SU2): Analysis and Design Technology for Turbulent Flows,” *52nd Aerospace Sciences Meeting*, jan 2014.
- ²⁰Palacios, F., Colonna, M., Aranake, A., Campos, A., Copeland, S., Economon, T. D., Lonkar, A., Lukaczyk, T., Taylor, T., and Alonso, J. J., “Stanford University Unstructured (SU2): An open-source integrated computational environment for multi-physics simulation and design,” *51st AIAA Aerospace Sciences Meeting including the New Horizons Forum and Aerospace Exposition*, jan 2013.
- ²¹Hirsch, C., *Numerical Computation of Internal and External Flows*, Wiley, New York, 1984.
- ²²Sutherland, W., “The viscosity of gases and molecular force,” *Philosophical Magazine Series*, 1893.
- ²³Weiss, J., Maruszewski, J., and Smith, W., “Implicit solution of the Navier-Stokes equations on unstructured meshes,” *AIAA paper*, Vol. 2103, 1997, pp. 139–149.
- ²⁴Forrester, A., Sobester, A., and Keane, A., *Engineering Design Via Surrogate Modelling: A Practical Guide*, Progress in Astronautics and Aeronautics, Wiley, 2008.
- ²⁵Pedregosa, F., Varoquaux, G., Gramfort, A., Michel, V., Thirion, B., Grisel, O., Blondel, M., Prettenhofer, P., Weiss, R., Dubourg, V., Vanderplas, J., Passos, A., Cournapeau, D., Brucher, M., Perrot, M., and Duchesnay, E., “Scikit-learn: Machine Learning in Python,” *Journal of Machine Learning Research*, Vol. 12, 2011, pp. 2825–2830.
- ²⁶Storms, B., Satran, D., Heineck, J., and Walker, S., “A Study of Reynolds Number Effects and Drag-Reduction Concepts on a Generic Tractor-Trailer,” *34th AIAA Fluid Dynamics Conference and Exhibit*, jun 2004.
- ²⁷Roy, C., Payne, J., McWherter-Payne, M., and Salari, K., “RANS Simulations of a Simplified Tractor/Trailer Geometry,” *Journal of Fluids Engineering*, Vol. 128, No. 5, 2006, pp. 1083–1089.
- ²⁸Towns, J., Cockerill, T., Dahan, M., Foster, I., Gaither, K., Grimshaw, A., Hazlewood, V., Lathrop, S., Lifka, D., Peterson, G. D., Roskies, R., Scott, J. R., and Wilkens-Diehr, N., “XSEDE: Accelerating scientific discovery,” *Computing in Science and Engineering*, Vol. 16, No. 5, 2014, pp. 62–74.